Cytoplasmic Molecular Delivery with Shock Waves: Importance of Impulse

Tetsuya Kodama, Michael R. Hamblin, and Apostolos G. Doukas
Wellman Laboratories of Photomedicine, Massachusetts General Hospital, and Department of Dermatology, Harvard Medical School, Boston, MA

ABSTRACT Cell permeabilization using shock waves may be a way of introducing macromolecules and small polar molecules into the cytoplasm, and may have applications in gene therapy and anticancer drug delivery. The pressure profile of a shock wave indicates its energy content, and shock-wave propagation in tissue is associated with cellular displacement, leading to the development of cell deformation. In the present study, three different shock-wave sources were investigated; argon fluoride excimer laser, ruby laser, and shock tube. The duration of the pressure pulse of the shock tube was 100 times longer than the lasers. The uptake of two fluorophores, calcein (molecular weight: 622) and fluorescein isothiocyanate-dextran (molecular weight: 71,600), into HL-60 human promyelocytic leukemia cells was investigated. The intracellular fluorescence was measured by a spectrofluorometer, and the cells were examined by confocal fluorescence microscopy. A single shock wave generated by the shock tube delivered both fluorophores into approximately 50% of the cells ($p < 0.01$), whereas shock waves from the lasers did not. The cell survival fraction was >0.95. Confocal microscopy showed that, in the case of calcein, there was a uniform fluorescence throughout the cell, whereas, in the case of FITC-dextran, the fluorescence was sometimes in the nucleus and at other times not. We conclude that the impulse of the shock wave (i.e., the pressure integrated over time), rather than the peak pressure, was a dominant factor for causing fluorophore uptake into living cells, and that shock waves might have changed the permeability of the nuclear membrane and transferred molecules directly into the nucleus.

INTRODUCTION

There are many situations in medicine and biology when it is desired to introduce a macromolecule into the cytoplasm of mammalian cells (Hapala, 1997). One important application is gene therapy, where it is necessary to deliver a gene or a synthetic oligonucleotide into the cell. Gene therapy has attracted attention as a possible solution to many major diseases such as cancer (Fueyo et al., 1999; Gutierrez et al., 1992), cardiovascular disease (Finkel and Epstein, 1995), and inherited metabolic disorders. Achieving the efficient delivery of a macromolecule to the cytoplasm and thence to the nucleus is inherently difficult, because the natural mechanism used by cells to take up macromolecules is endocytosis. All three variants of endocytosis (receptor-mediated, adsorptive, and fluid-phase) lead to the endosomal–lysosomal pathway, and exposure of the macromolecule to many degradative enzymes such as nucleases, proteases, etc. (Mukherjee et al., 1997). Other important applications of intracellular macromolecular delivery include the use of ribosome-inactivating proteins in cancer therapy (Barbieri et al., 1993) and the elucidation of cellular metabolic pathways by the introduction of active biomolecules (Cockcroft, 1998).

Received for publication 10 December 1999 and in final form 7 July 2000.

Address reprint requests to Tetsuya Kodama, Harvard Medical School, Massachusetts General Hospital, Department of Dermatology, Wellman Laboratories of Photomedicine, 55 Fruit Street - WEL 224, Boston, MA 02114. Tel.: 617-724-2881; Fax: 617-726-3192; E-mail: kodama@helix.mgh.harvard.edu.

0006-3495/00/10/1821/12 $2.00

Cells take up small polar molecules either by specific transmembrane transporters (Cass et al., 1998), or by fluid-phase endocytosis (Connelly et al., 1993). The first process has a high degree of structure specificity, whereas the second has a low capacity. There are applications where a method of increasing the cellular uptake of small polar molecules would be desirable, e.g., potentiating the effects of cisplatin (Weiss et al., 1994) and bleomycin (Kambe et al., 1996) in cancer therapy.

Many methods have been devised to produce the transient permeabilization of cells without concomitant cytotoxicity. These include the use of detergents such as digitonin that alter membrane lipid structure (Schafer et al., 1987), bacterial toxins such as Streptolysin O (Spiller et al., 1998), virus-mediated fusogenic liposomes (Kaneda, 1999), the use of pulsed electric fields (electroporation) (Ho and Mittal, 1996), the use of ultrasound (sonoporation) (Liu et al., 1998; Miller et al., 1999). Another method that may be applicable is the use of shock waves generated by extracorporeal lithotripters (Delius and Adams, 1999; Gambihler et al., 1994) or lasers (Lee and Doukas, 1999). The increase of membrane permeability due to the application of shock waves generated by a lithotripter was first demonstrated by inducing L1210 mouse leukemia cells to take up propidium iodide (Gambihler and Delius, 1992a) and fluorescein isothiocyanate dextran (FITC-D, molecular weights up to 2,000,000 (Gambihler et al., 1994).

Shock waves are nonlinear and finite-amplitude waves, and the flow induced behind the shock waves cannot be ignored. The duration time of the particle motion is the order of the pulse duration, dt, of the shock wave, and the displacement, d, of the particle is about the order of $d =$

$u_p \times dt$, where u_p is the induced speed, which is inversely proportional to the density of the particle. A rough estimate of tissue displacement obtained with a single shock wave generated by a clinical lithotripter is calculated to be 1–20 μm, using pressure data obtained in water (Coleman and Saunders, 1989). This value is similar to that (7–10 μm) measured in rabbit liver resulting from a shock wave produced by detonation of an explosive micropellet (Kodama et al., 1998). Transmembrane molecular delivery depends on the shock wave pressure profile, but little is known about the relationship between the pressure profile and the delivery mechanism.

In the present paper, three different shock wave sources, excimer laser, ruby laser, and shock tube were used to investigate the relationship between the pressure profile and the uptake of fluorophores into HL-60 human promyelocytic leukemia cells.

MATERIALS AND METHODS

Cell preparation

Human promyelocytic leukemia cells (HL-60) were obtained from the American Type Culture Collection (ATCC) (Rockville, MD), and were cultured in suspension in RPMI-1640 medium (Life Technologies Inc., Grand Island, NY) with 20% fetal bovine serum (Life Technologies Inc.) in 750-ml flasks (Fisher Scientific Co., Pittsburgh, PA) in a cell culture incubator (Model 2720, Queue, Parkersburg, WV) at 37°C under an atmosphere of 5% CO_2 in air. Total cell counts and the viability were counted in a hemocytometer (Hausser Scientific, Horsham, PA) with the trypan blue dye exclusion method (Tennant, 1964) before and after the shock wave experiments. Only cells in the exponential growth phase, with ≥95% viability, were used. In the experiments using the excimer and ruby lasers, polystyrene tubes constructed from 55-mm lengths cut from 1 ml serological pipettes 3 mm in diameter (Becton Dickinson, Franklin Lakes, NJ) sealed at one end with a polystyrene plate (thickness 2.2 mm) were used as test tubes. For the shock tube experiments, flat-top snap-cap micro-centrifuge tubes (Fisher Scientific Co., 7.5 mm outer diameter, 30.5 mm length, 0.5 ml) were used. The centrifuge tube was covered with a triple layer of Parafilm (Parafilm "M", American National Can, Chicago, IL). Both test tubes were filled with a mixture of the fluorophore solution (200 μM) and 2.0×10^6 cells in serum-containing medium. A cell pellet was gently formed by centrifugation (5 min at $233 \times g$). Because endocytosis is a temperature-dependent process (Basrai et al., 1990), the test tubes were kept in an ice bath at 0.5°C except during a brief period of time during the application of shock waves to reduce the potential of uptake of the fluorophore due to endocytosis.

Fluorophores

Calcein (622 Da) (Sigma, St. Louis, MO; absorption 496 nm, emission 514 nm) and fluorescein isothiocyanate-dextran (FITC-D, 71600 Da) (Sigma, absorption 494 nm, emission 514 nm) were used for evaluation of the uptake of molecules by the cells. Solutions of the fluorophore at a concentration of 200 μM were prepared in phosphate-buffered saline without Mg^{2+} and Ca^{2+} (PBS). Propidium iodide (PI) (Molecular Probes, Eugene, OR; absorption 535 nm, emission 617 nm) was added to the cells to give a final concentration of 20 μg/ml 5 minutes before confocal microscopy to distinguish between living and damaged cells before capturing the confocal images.

Laser generation of shock waves

An argon fluoride (ArF) excimer laser (wavelength 193 nm, pulse duration full width at half maximum 14 ns) (Excimer laser LPX 300cc, Lambda Physics Inc., Acton, MA) and a Q-switched ruby laser (wavelength 694.3 nm, pulse width 28 ns) (model RD-1200, Spectrum Medical Technologies Inc., Natick, MA) were used. The laser fluence was 2.5 and 5.5 J cm^{-2} for the excimer laser, and 17.3, 28.8, and 40.3 J cm^{-2} for the ruby laser. Figure 1 *A* shows the experimental arrangement. The laser beam was delivered to the polystyrene plate sealing the bottom of the test tube as a focused 3-mm-diameter spot by way of a lens and a prism.

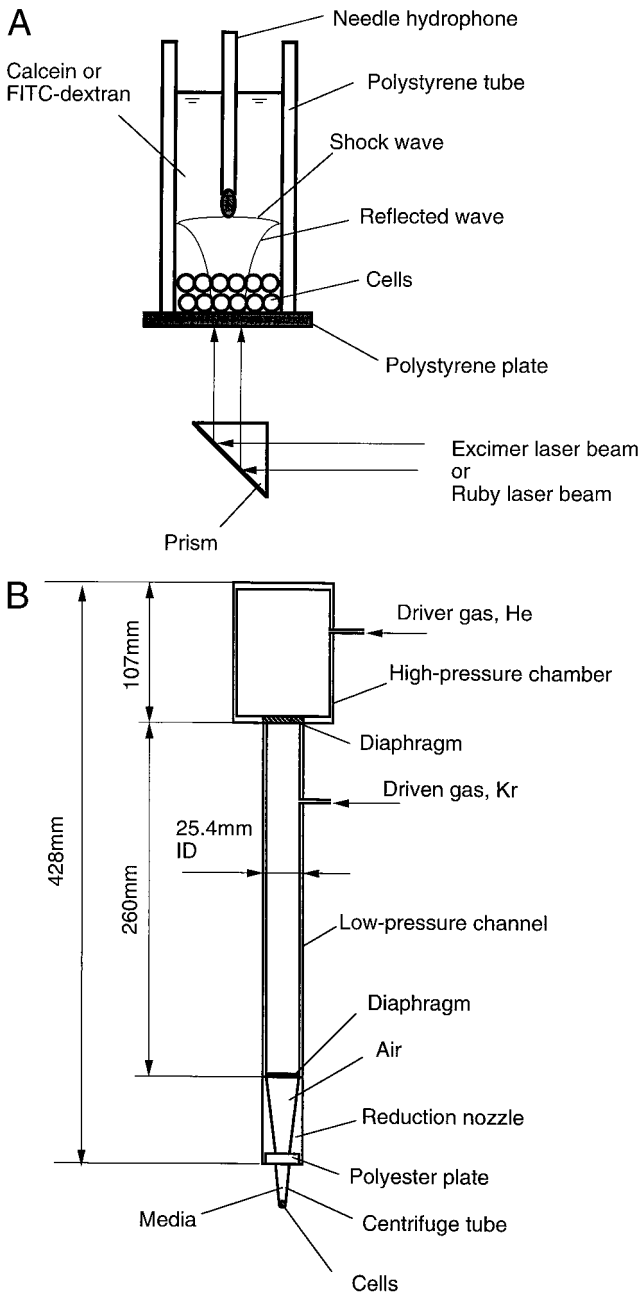

FIGURE 1 Schematic diagram of experimental setup. (*A*) Laser-generated shock wave permeabilization of cells. (*B*) Shock tube-induced permeabilization of cells.

Shock tube

The double diaphragm shock tube (Hall, 1958) was obtained from Pharma Wave (Boston, MA). It consisted of a high-pressure chamber (107 mm long), a low-pressure channel (260 mm long, 25.4 mm inner diameter), a reduction nozzle having a half-angle of 11.7° (Fig. 1 *B*). The high-pressure chamber was separated from the low-pressure channel with two adjacent diaphragms (thickness 0.127 mm, Part No. 44535, Precision Brand Product, Inc., Downers Grove, IL), and the low-pressure channel was separated from the reduction nozzle with one diaphragm (thickness 3.18 mm, Part No. 44550, Precision Brand Products, Inc.). A 0.5-ml microcentrifuge tube without the cap was covered with a plate made of terephthalate (diameter 25.4 mm, thickness 7.8 mm), and both were fitted to the reduction nozzle by screwing on the end fitting. Both the high-pressure chamber and the low-pressure channel were placed under a vacuum (4 kPa), and the former was filled with helium as the driver gas, whereas the later was filled with krypton as the driven gas. The pressure in the high-pressure chamber, P_2, was 1.2 MPa or 2.8 MPa. The pressure in the low-pressure channel, P_1, was fixed to 0.1 MPa. When the diaphragm placed between the high-pressure chamber and the low-pressure channel was ruptured by the pressure difference, the shock wave and the following high-velocity flow propagated from the diaphragm into the low-pressure channel. Based on an assumption of one-dimensional isentropic flows (Liepman and Roshko, 1957), the shock pressure, P_S, and the shock Mach number, M_S, in the low-pressure chamber were $P_S = 1.2$ MPa and $M_S = 3.1$ for $P_2 = 2.8$ MPa; and $P_S = 0.69$ MPa and $M_S = 2.4$ for $P_2 = 1.2$ MPa. The traveling shock wave then ruptured the second diaphragm, and converged into the microcentrifuge tube. The shock wave intensity in the microcentrifuge tube was increased by a factor of ~20 compared to the calculated pressure in the low-pressure channel.

Pressure measurements

A PVDF needle hydrophone (model 80-0.5-4.0, Imotec Messtechnik, Warendorf, Germany) with a 0.5-mm-diameter sensitive element, which gave an output of 0.0136 μV Pa^{-1}, positioned inside the test tube, was used to monitor the overpressure of the shock wave by changing the stand-off distance between the polystyrene plate and the hydrophone for the experiment with laser beams. The sensitivity was constant up to 10 MHz, the rise time was about 100 ns and it had registrations within the limits set out in IEC Standard 61846 (IEC, 1998). For the shock tube experiment, the hydrophone was placed on the bottom of the centrifuge tube. Measured data were stored and displayed on a digitizing oscilloscope (9360, 600 MHz, 1 MΩ [15 pF], LeCroy Co., New York, NY).

Fluorescence measurement

Measurements were performed in a spectrofluorometer (FluoroMAX™, Spex Industries Inc., Edison, NJ). Fluorescence emission was scanned from 490 to 600 nm at 20°C, after excitation at 496 nm (calcein) or 494 nm (FITC-D) with 1-nm-wide slits. The accuracy of the excitation wavelength was ±0.5 nm. All cell samples were washed with PBS (5 ml, 3×) to remove excess extracellular fluorophore and centrifuged (5 min at 233 × *g*). After three washes, the recovery rate of the cells was between 98% and 59%. The cell pellet was then resuspended in 3 ml PBS, counted with the hemocytometer, and transferred to a 10-mm square polystyrene cuvette (Fisher Scientific Co.). Each experiment consisted of 5 samples receiving fluorophore and shock wave and 5 control samples receiving fluorophore but no shock wave. For each experiment, the mean fluorescence of the treated samples was divided by the mean fluorescence of control samples to give a normalized fluorescence uptake. The mean of 3–10 values of normalized fluorescence uptakes was calculated for each shock wave source (ArF, ruby, and shock tube) and fluorophore (calcein and FITC-D).

Confocal fluorescence microscopy

Confocal fluorescence microscopy was performed on a confocal microscope (model DMRBE, Leica Microsystems, GmbH, Heidelberg, Germany) equipped with an 18-mW argon laser (model 2211-65ML, Uniphase, San Jose, CA). A 40× oil-immersion objective lens (PL AP0, Leica Microsystems) with a numerical aperture of 1.25 was used. Calcein, FITC-D, and PI fluorescence were excited with the 488-nm line of the argon laser. The laser excitation beam was directed to the specimen through a 488-nm dichroic beam splitter. Emitted fluorescence was collected through a 525–550-nm bandpass emission filter for the green channel and a 590-nm long pass filter for the red channel. Computer-generated images of 1-μm optical sections were taken at the geometric center of the cell as determined by repeated optical sectioning. The percentage of fluorescent cells for each sample was calculated by examining 3–6 fields each containing 10–100 cells. Both weakly and strongly fluorescent cells were counted as positive. Means of 3–5 samples were calculated to give final percentage of fluorescent cells.

Statistical analysis

All measurements are given as mean ± standard deviation (SD). Values are the means of 3–10 separate experiments with an average of five samples per experiment. Differences between all samples were assessed by one-way factorial ANOVA. A value of $p < 0.05$ was considered to be statistically significant.

RESULTS

Pressure profiles

Figure 2 shows three pressure waveforms measured in water, that were generated with the excimer laser, ruby laser, and shock tube. The fluences of the excimer and ruby laser beams were 5.5 J cm^{-2} and 40.3 J cm^{-2}, respectively. For the shock tube, $P_2 = 2.8$ MPa and $P_1 = 0.1$ MPa. The standoff distance between the hydrophone and polystyrene plate was 0.5 mm for the excimer and ruby lasers. When the polystyrene plate was exposed to the laser beam under a condition of stress confinement, stress waves were generated in the polystyrene (Frenz et al., 1996; Bushnell and McCloskey, 1968). The stress waves became bipolar when the polystyrene surface exposed by the laser beam was in contact with air because of the acoustic mismatch between polystyrene and air (Fig. 2 *a*). The bipolar stress waves propagated in polystyrene and were transmitted into water. A part of the stress wave was reflected back at the interface of the water, was reflected again at the other side facing the air, and was transmitted to the water. The second peak pressure observed 1.86 μs after the first peak pressure was the result of the above reflection process (Fig. 2 *a*). The thickness of the polystyrene was 2.2 mm. Therefore, the wave velocity in the polystyrene was calculated to be 2366 m s^{-1}, which was close to 2350 m s^{-1} reported in a database (Lide, 1999). The cells were mainly affected by the first shock wave, because the intensity of the second shock wave was negligible compared with that of the first.

For the ruby laser (Fig. 2 *b*), the positive and negative waves, and the reflected waves were recorded. The compo-

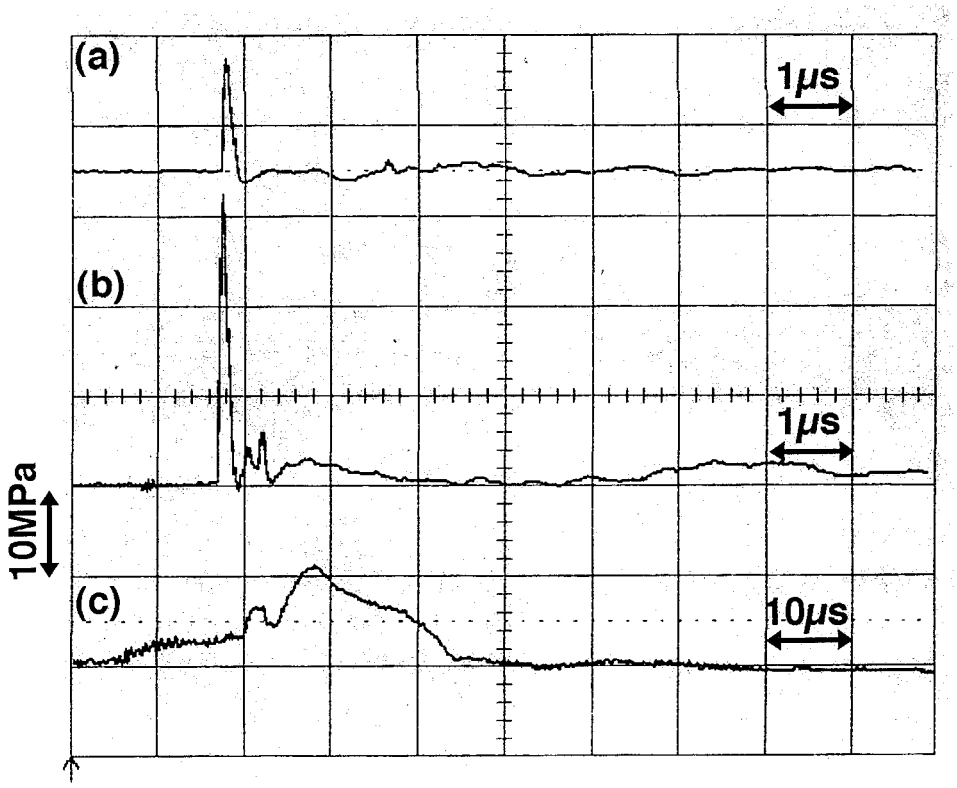

FIGURE 2 Pressure wave profiles for the excimer laser, ruby laser, and shock tube. (*a*) Excimer laser, 5.5 J cm^{-2}; (*b*) Ruby laser, 40.3 J cm^{-2}; (*c*) Shock tube gas pressures, P_2 = 2.8 MPa, P_1 = 0.1 MPa.

nent of the negative phase of the ruby laser was less than that produced by the excimer laser because the fluence of the laser beam was larger than that of the excimer laser by a factor of 7.3, resulting in greater ablation of the polystyrene. The reflections of the transmitted shock wave at the inside wall were clearly observed in the case of the ruby laser, compared with the excimer laser. This was due to the different pressure waveform resulting from less uniform energy distribution over the laser focus area. The pulse duration of the shock wave generated by the shock tube was longer than those of pulses of the excimer and ruby lasers by a factor of 100 (Fig. 2 *c*).

Table 1 shows pressure parameters generated by three shock-wave sources. The values of peak pressures P_+, P_-, the rise time of the first positive half-cycle, t_r, the durations of the first positive and first negative half-cycles, t_+ and t_-, the impulse, I, integrated for t_+, respectively, are given in Table 1. The rise time for the shock tube was not determined because the rise profile of the waveform was nonlinear due to the reflected waves generated in the shock tube. The

TABLE 1 Shock wave parameters

	Condition	P_+ (MPa)	P_- (MPa)	t_r (ns)	t_+ (ns)	t_- (ns)	I (Pa·s)
ArF laser	2.5 J cm^{-2}	8.3 ± 0.0	0.96 ± 0.1	37.8 ± 0.8	178.8 ± 16	217.7 ± 3.0	0.7 ± 0.1
	5.5 J cm^{-2}	12.4 ± 0.0	1.2 ± 0.1	38.5 ± 0.7	196.3 ± 2.9	211.8 ± 2.3	1.1 ± 0.0
Ruby laser	17.3 J cm^{-2}	20.1 ± 2.1	0.4 ± 0.0	42.1 ± 2.6	178.0 ± 4.7	11.8 ± 2.3	2.5 ± 0.2
	28.8 J cm^{-2}	24.1 ± 1.2	0.45	39.0 ± 0.7	195.5 ± 4.3	44.5	3.1 ± 0.1
	40.3 J cm^{-2}	31.9 ± 0.0	0.78 ± 0.0	34.8 ± 0.2	202.7 ± 1.9	49.3 ± 3.3	4.0 ± 0.1
Shock tube	P_2 = 1.2, P_1 = 0.1 MPa	3.4 ± 1.1	0.91 ± 0.32	—	23700 ± 4000	35770 ± 19350	54.1 ± 8.9
	P_2 = 2.8, P_1 = 0.1 MPa	11.6 ± 1.6	2.16 ± 0.22	—	32100 ± 7100	10700 ± 4100	141.8 ± 24.4

Positive and negative peak pressures, P_+ and P_-, rise time t_r and positive and negative half cycle durations, t_+ and t_-, impulse, I integrated for t_+, over a range of energy densities of the excimer and ruby laser beams, and the gas pressure ratio of the shock tube. The rise time was defined as the time required for pressure to increase from 10% to 90% of the maximum positive value. The rise time for the shock tube was undetermined because the rise characteristic of the waveform was nonlinear due to the reflected waves generated in the shock tube. Shock-wave parameters were measured by a PVDF needle hydrophone. Values are the mean of 3 measurements and are ±SD.

maximum pressure measured was 31.9 MPa, which was obtained by the ruby laser at a fluence of 40.3 J cm^{-2}.

Using one-dimensional momentum equations (Balhaus and Holt, 1974), the shock Mach number, M_S, the induced particle speed, u_p, and the density, ρ, of the water behind the shock wave with a pressure of 31.9 MPa, were determined to be 1.03, 19.8 m s^{-1}, and 1011.4 kg m^{-3} respectively, where the sound speed in water is 1482 m s^{-1}, the atmospheric pressure was 101.3 kPa, and the water temperature was 20°C, giving a value for density of 998.2 kg m^{-3}. Because the shock wave velocity was very close to the acoustic limit ($M_S = 1.03$) and the density increase was only 1%, both the cells and surrounding liquid were treated as an incompressible fluid in the present paper.

Uptake of fluorophore in surviving cells

Table 2 shows the mean normalized fluorescence uptake, the percentage of permeabilized cells, and the survival fraction of the cells exposed to a single shock wave in the presence of FITC-D or calcein. The values in the column headed Pressure are the positive pressure values generated by each shock wave source; the intensity of the negative pressure was small or negligible compared to the positive pressure (see Table 1). Only shock waves delivered by the shock tube caused a significant increase in mean normalized fluorescence uptake for both fluorophores. In the case of FITC-D this was significant for a pressure of 11.6 ± 1.6 MPa (mean normalized fluorescence uptake = 3.95 ± 2.32, $p = 0.01$), whereas, for calcein, both the pressures (3.4 ± 1.1 and 11.6 ± 1.6 MPa) caused significant increases in mean normalized fluorescence uptake (1.53 ± 0.23, $p < 0.05$ and 4.28 ± 1.84, $p < 0.01$, respectively). None of the shock waves produced by the laser pulses produced any significant increases in mean normalized fluorescence uptake. The cell viability, as measured by the survival fraction, was not significantly affected by any shock waves except that from the shock tube at 11.6 ± 1.6 MPa in the presence of FITC-D where there was a small but significant reduction to 0.97 ± 0.02 compared to control, $p = 0.03$. It was clear that the uptake of the fluorescence in surviving cells was independent of the peak pressure value.

To confirm that the fluorophores actually entered the cytoplasm, confocal microscopy was used to provide thin optical sections through living cells. Figure 3 shows differential-interference-contrast (*a*, *c*, *e*, *g*, *i*) and fluorescence (*b*, *d*, *f*, *h*, *j*) images of representative living HL-60 cells exposed to a single shock wave; calcein (*a*, *b*, *c*, *d*) and FITC-D (*e*, *f*, *g*, *h*, *i*, *j*). The pressure was 11.6 ± 1.6 MPa, generated by the shock tube. Propidium iodide was used in some preparations to confirm that the cells that took up fluorophores were still alive and excluded PI. Control samples showed only a weak fluorescence due to a small uptake of the fluorophore (Fig. 3, *b* and *f*). The samples treated with shock wave in the presence of calcein showed intense fluorescence uniformly distributed throughout the whole cell (Fig. 3 *d*). Not all cells showed fluorescence; the proportion of fluorescent cells was 47.1 ± 18.7% (9 fields of

TABLE 2 Results of cell permeabilization experiments

		FITC-D (71.6 kDa)			Calcein (622 Da)		
	Pressure P_+ (MPa)*	Mean Normalized Fluorescence Uptake†	% Cells Permeabilized‡	Survival Fraction§	Mean Normalized Fluorescence Uptake†	% Cells Permeabilized‡	Survival Fraction§
ArF laser	8.3 ± 0.0	0.97 ± 0.13		1.01 ± 0.00	1.04 ± 0.23		1.01 ± 0.02
	12.4 ± 0.0	0.87 ± 0.38		1.00 ± 0.01	1.04 ± 0.25		0.99 ± 0.01
Ruby laser	20.1 ± 2.1	0.95 ± 0.42		1.00 ± 0.02	0.99 ± 0.14		1.00 ± 0.02
	24.1 ± 1.2	0.77 ± 0.27		1.00 ± 0.01	1.07 ± 0.22		1.00 ± 0.02
	31.9 ± 0.0	0.94 ± 0.18		1.00 ± 0.02	1.31 ± 0.27		1.00 ± 0.01
Shock tube	3.4 ± 1.1	1.35 ± 0.24	n.d.	1.00 ± 0.00	1.53 ± 0.23 ($p < 0.05$)	n.d.	1.00 ± 0.01
	11.6 ± 1.6	3.95 ± 2.32 ($p = 0.01$)	43.7 ± 10.7	0.97 ± 0.02 ($p = 0.03$)	4.28 ± 1.84 ($p < 0.01$)	47.1 ± 18.7	0.98 ± 0.02 ($p > 0.05$)

n.d. = not determined.

*Positive pressure measured by a PVDF needle hydrophone. Mean of 3–4 determinations ±SD.

†Mean normalized fluorescence uptake. Each experiment consisted of five samples receiving fluorophore and shock wave and five control samples receiving fluorophore but no shock wave. For each experiment, the mean fluorescence of the treated samples was divided by the mean fluorescence of control samples to give a normalized fluorescence uptake. The mean of 3–10 values of normalized fluorescence uptakes was calculated for each shock-wave source and fluorophore. Values are ±SD.

‡The percentage of fluorescent cells for each sample was calculated by examining 3–6 fields each containing 10–100 cells. Both weakly and strongly fluorescent cells were counted as positive. Means of 3–5 samples were calculated to give final percentage fluorescent cells, values are ±SD.

§Survival fraction measured by trypan blue dye-exclusion method and counting in a hemocytometer before and after the shock-wave experiments. Each experiment consisted of five samples receiving fluorophore and shock wave and five control samples receiving fluorophore but no shock wave. For each experiment, the mean percentage of trypan blue-excluding cells in the treated samples was divided by the mean percentage of trypan blue-excluding cells in the control samples to give a survival fraction. The mean of 3–10 survival fractions was calculated for each shock wave source and fluorophore. Values are ±SD.

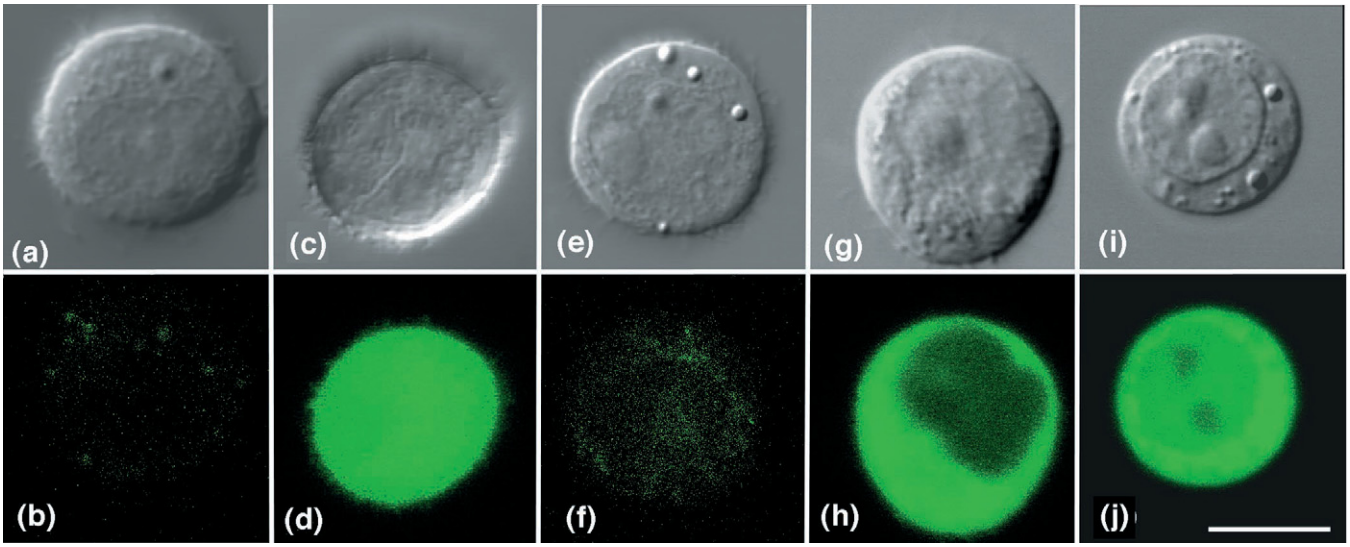

FIGURE 3 Differential-interference-contrast (*a*, *c*, *e*, *g*, *i*) and fluorescence (*b*, *d*, *f*, *h*, *j*) confocal images of representative living HL-60 cells exposed to a single shock wave in the presence of 200 μM; calcein (622 Da) (*a*, *b*, *c*, *d*) and FITC-dextran (71.6 kDa) (*e*, *f*, *g*, *h*, *i*, *j*). Fluorescence was excited with the 488-nm line of the argon laser and collected through a 525–550-nm bandpass emission filter. The sections were taken at the geometric center of the cell. The shock wave pressure was 11.6 $\pm$ 1.6 MPa (n = 4), generated by the shock tube. The samples were washed three times with PBS. Scale bar indicates 10 μm.

cells) for calcein. For cells treated with a shock wave in the presence of FITC-D, there were three types of fluorescence images obtained. The nonfluorescent cells (Fig. 3 *f*) comprised 56.3 $\pm$ 10.7% of the total (17 fields of cells) (Table 2). The remaining fluorescent cells could have one of two appearances. The first shown in Fig. 3 *h* has the nucleus dark compared to the evenly stained cytoplasm, whereas the second shown in Fig. 3 *j* shows the nucleus to be intermediately stained, whereas the nucleoli are less bright but still have some fluorescence. The procedure for imaging consisted of eight confocal sections separated by 1 μm, so it is unlikely that these images were the result of the confocal microscope missing a dark nucleus. Observed with differential-interference-contrast, fluorescence-retaining cells exposed to the shock wave were indistinguishable from the unshocked cells (Fig. 3, *a*, *c*, *e*, *g*, and *i*).

Each shock wave source generated a different shock waveform, so it is uncertain precisely which shock wave parameters were important for uptake of the fluorophore. Because the fluorophore uptake did not depend on the peak pressures of the shock waves, we investigated uptake as a function of the impulse *I*. The impulse is denoted by

$$I = \int_0^{t_+} p(t)\,\mathrm{d}t, \qquad (1)$$

where $p(t)$ is the shock wave pressure, and t_+ is the positive phase duration of a half-cycle of the shock wave (see Table 1).

Figure 4 shows the relationship between the mean normalized fluorescence uptake and the impulse. The uptake of the fluorophore occurred only after shock tube permeabilization. No fluorophore was taken up when either the excimer or the ruby laser was used to generate the shock wave (see Table 2). The intensity of the intracellular fluorescence increased with increasing impulse. The results suggest that

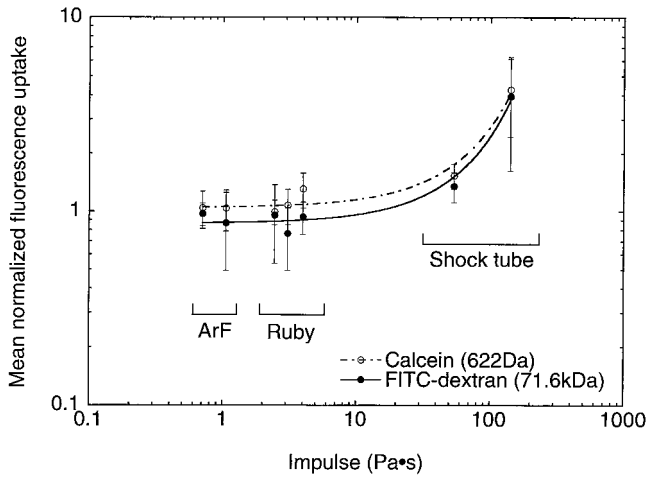

FIGURE 4 Relationship between the mean normalized fluorescence uptake and the impulse of the shock wave for each shock-wave source. The fluorophores were calcein (622 Da) and FITC-D (71.6 kDa). Each experiment consisted of five samples receiving fluorophore and shock wave and five control samples receiving fluorophore but no shock wave. For each experiment, the mean fluorescence of the treated samples was divided by the mean fluorescence of control samples to give a normalized fluorescence uptake. The mean of 3–10 values of normalized fluorescence uptakes was calculated for each shock-wave source and fluorophore. Error bars indicate SD.

there is a threshold value of the impulse for causing uptake of fluorophore.

DISCUSSION

We have shown that shock waves are capable of delivering large molecules into the cytoplasm of cells without causing significant cytotoxicity. It was found that the uptake of the fluorophore by the cells was closely related to the impulse of the shock wave (see Fig. 4). We shall attempt to define the physical significance of the factors involved. Consider the one-dimensional wave propagation in the liquid including and surrounding the cells. Because the modulus of compressibility of the liquid due to the shock wave pressure in the present case is negligible (see Results section, Pressure profiles), we can assume that the liquid and cells together is an incompressible fluid. Suppose that all the cells are the same size and are uniformly distributed in the liquid. When an impulsive wave propagates into the liquid, the sudden relative displacement, d, and the difference in the kinetic energy density values, ε, between the cell and liquid phases are given by (see Eq. A18 and Eq. A19)

$$d = \left| \frac{I}{\rho_m U_m} [\alpha(\beta - 1) + 1] \left[\left(1 + \frac{1}{\beta} \right) \alpha - 1 \right] \right|, \quad \beta = \frac{\rho_c}{\rho_f}, \tag{2}$$

$$\varepsilon = \left| -\frac{1}{2} \frac{I^2}{\rho_m U_m^2 t_+^2} [\alpha(\beta - 1) + 1] \left[\left(1 + \frac{1}{\beta} \right) \alpha - 1 \right] \right|, \tag{3}$$

where I is defined in Eq. 1, ρ_m is the average density of the liquid including cells, ρ_f is the density of the liquid phase, ρ_c is the density of the cell phase, β is the ratio of ρ_c to ρ_f, α is the cellular volume fraction (the fraction of the total volume occupied by cells) varying from 0 to 1, t_+ is defined in Table 1, and U_m is the wave velocity of the liquid with cells which is defined by Eq. A17.

Figure 5 shows that the relationship between the cellular volume fraction and relative displacement for different impulse values given in Table 1, where β has been chosen to have a value of 1.1. This value was close to the value of the ratio of the density of normal erythrocytes to the density of water found to be 1.09 (Schwartz et al., 1998). The relative displacement has a minimum value around $\alpha = 0.5$, and increases as α approaches 0 and also as α approaches 1. The curves increase with increasing impulse. The nonsymmetry of the curves with respect to the y-axis around $\alpha = 0.5$ is due to $\beta > 1$.

In the experiment, HL-60 cells were centrifuged to form a cell pellet at the bottom of the tube. Assume HL-60 cells have a constant spherical shape having a circular cross-section with a diameter of 10 μm, then the cellular volume fraction of the pellet is calculated to be $\alpha = 0.67$. In addition, the density of each fluorophore is assumed to be equal to that of liquid, because each compound is highly

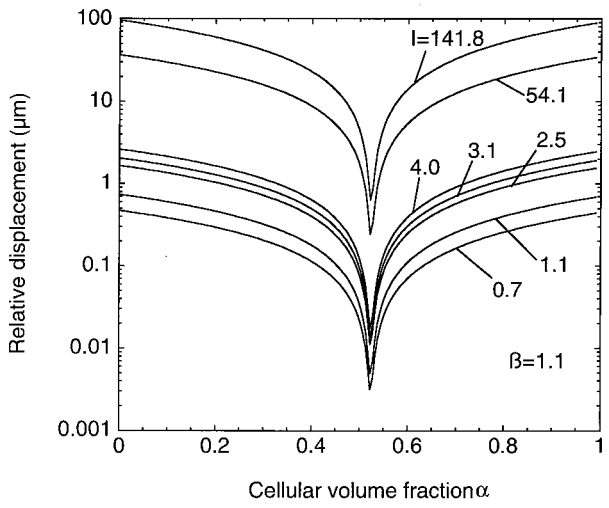

FIGURE 5 Relationship between the cellular volume fraction and relative displacement for different impulse values, I, given in Table 1. β is the ratio of the density of the cell phase to that of the liquid phase.

hydrophilic and characterized by good water solubility. Therefore, the molecules move in the direction of the shock wave, with the same speed and distance as those of the liquid molecules when shock waves move into the liquid. At $\alpha = 0.67$, the displacements for the excimer ($I = 0.7$, 1.1 Pa·s) and ruby lasers ($I = 2.5$, 3.1, 4.0 Pa·s) were calculated to be less than 1 μm. Whereas, for the shock tube ($I = 54.1$, 141.8 Pa·s), the displacement was calculated to be about 20 μm at $I = 54$ Pa·s, and about 30 μm at $I = 141$ Pa·s (see Fig. 5), which is greater than the diameter of the cells. The uptake of calcein occurred at $I = 54$ Pa·s, and the uptake of both calcein and FITC-D occurred at $I = 141$ Pa·s (see Table 2).

Stokes radius is the effective radius of a molecule that depends on the molecular weight and molecular configuration and has been used as a determinant of transport through biological matrices (Bohrer et al., 1979). Stokes radii for the calcein and FITC-D were estimated to be 0.68 nm, and 6.2 nm using reported data, respectively (Curry et al., 1983; Fox and Wayland, 1979; Gambihler et al., 1994; Nugent and Jain, 1984). Thus, the uptake of fluorophore depends on the impulse and possibly also on the molecular weight. The uptake dependency on the applied physical force was observed in electroporation (Mir et al., 1988), and the molecular size dependency was reported in the permeabilization of cells to large molecules using a lithotripter (Gambihler et al., 1994), and also in electroporation of cells (Glogauer and McCulloch, 1992). From Fig. 5, the relative displacement increases when α reaches 0 or 1. Thus, we can expect that the uptake of fluorophore may occur if cells are widely separated ($\alpha \to 0$) or packed together ($\alpha \to 1$). When $\alpha \to 0$, there are too few cells to allow efficient permeabilization. Therefore, the tightly packed state is likely to give the most effective permeabilization.

Figure 6 shows the difference in the kinetic energy density between the cell and liquid phases for different impulse values, where $\alpha = 0.67$ and β is varied from 1 to 1.3. The difference in the kinetic energy density between the ruby laser and both the excimer and shock tube was large, whereas the difference between the values of kinetic energy density for the excimer laser and shock tube was much smaller. The difference in the energy density for each shock source, however, was not found to be an important factor for the cell uptake. That is, a waveform with a long pulse duration may have the potential to increase the efficiency of cytoplasmic molecular delivery even though it has a lower pressure value. Variations in β do not have a significant effect on the kinetic energy density difference values.

In geometrically similar flows, the viscous force against a body whose characteristic length L in a flow with characteristic velocity U is proportional to μUL where μ = coefficient of viscosity. Thus, the viscous force against cells increases in proportion to the difference in the velocity between the cell and liquid phases, which is proportional to the increase in relative displacement between the phases (see Fig. 5). Therefore, the shear force at the cell surface may change the permeability of the cell membrane.

This mathematical model has the following limitations; the inertia term $(\mathbf{v} \cdot \text{grad})\mathbf{v}$ and the viscosity term $\mu\Delta\mathbf{v}$ were omitted because the duration of the impulse pressure was assumed to be infinitesimal, therefore, the local derivative $\partial\mathbf{v}/\partial t$ becomes dominant. In addition, the shape of cell was assumed to remain constant and the flow field was assumed to be one-dimensional. Furthermore, the pressure field in the test tube was not uniform due to the three-dimensional shape of the test tube and subsequent wave reflections (see Fig. 2). The omitted terms will have finite values with

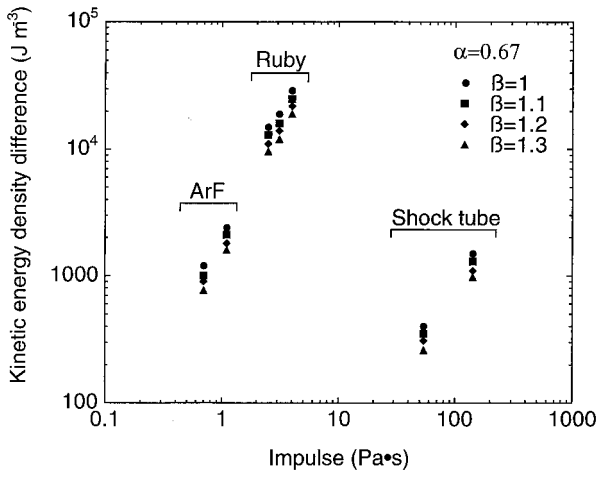

FIGURE 6 Difference between the kinetic energy density values of the cell and liquid phases at $\alpha = 0.67$ for different impulse values. The impulse for the excimer laser, ruby laser, and shock tube is given in Table 1. β is the ratio of the density of the cell phase to that of the liquid phase, which is assumed to vary from 1 to 1.3.

increasing pulse duration, resulting in viscous stress occurring in the moving fluid, and shear stress between the cell and liquid phases. The subsequent cell deformation at different times and positions due to varying shear stresses may account for the numerical distribution of fluorescent cells obtained in the experiment. If the impulse increases, the percentage of fluorescent cells may increase. Because it was reported that there was a relationship between the electric field intensity and number of fluorescent cells in electropermeabilization (Mir et al., 1988), there may be values of the shock wave impulse that will increase the percentage of fluorescent cells.

Eucaryotic cells contain a rich array of intracellular organelles with different densities and containing varying amounts of internal membranes. The cytoskeleton provides the mechanism to maintain the shape and control the basic movement of cells. The behavior of a cell can be thought of as that of a viscoelastic material (Fung, 1993). Because intracellular organelles may have different densities, the shock wave will cause the less dense organelles to move preferentially, thus adding to the deformation experienced by the cell. The cell membrane was found to be the most sensitive to the shock wave propagation among the cell components (Steinbach et al., 1992). Because each cell line may show differences in intracellular densities and fluidities of membranes, the value of the shock wave-induced surface viscosity may be different for each cell line, leading to different membrane permeability.

Our confocal fluorescence micrographs showed that the small molecule calcein is readily taken up by the nucleus of HL-60 cells after its introduction into the cytoplasm by shock waves. This is in agreement with data using the dye lucifer yellow (457 Da, Stokes radius = 0.59 nm) where Mir et al. (1988) showed that electropermeabilization produced very similar images with uniform nuclear fluorescence. Paine et al. (1975) have calculated that molecules with a radius less than 4.5 nm have no barrier to intranuclear transport. Our fluorescence micrographs with FITC-D showed that some of the permeabilized cells appear to have fluorophore in the nucleus while others do not. Many workers have investigated the permeability of the nuclear membrane, and have studied the size dependence of molecular transport through the nuclear pore complexes. Peters (Peters, 1984) found that FITC-D of molecular weight 20,000 (Stokes radius 3.3 nm) but not 70,000 (Stokes radius 5.5 nm) penetrated the nucleus. Schindler and Jiang (1986) found that 64-kDa dextran had a significant nuclear uptake. It has been proposed that the effective diameter of the nuclear pore can vary among cell types and, in the same cell type, between different stages of the cell cycle (Paine et al., 1975).

Other workers have studied the permeabilization of cells in vitro by shock waves. Gambihler et al. (1994) have used an extracorporeal shock wave lithotripter to permeabilize cells to macromolecular FITC-D (molecular weights up to

2,000,000) using 250 shots with a pressure of 50 MPa (Coleman and Saunders, 1989). They showed (Gambihler et al., 1994) the increase in the uptake of FITC-dextran of 35.6 kDa by a factor of 4 with 250 lithotripter-induced shock waves. The viability was about 50%. Miller et al. (1998) showed that, using FITC-dextran of 580 kDa, the percent of the fluorescent cells was about 50% and the survival fraction was about 0.2 after 1000 shock waves. In the present paper, we used a single shock wave, which showed the increase in the uptake by a factor of 4, the percent of the fluorescence cells was ~50% and the survival fraction is close to 1. Recently, it was reported (Delius and Adams, 1999) that the use of this procedure could permeabilize cancer cells to ribosome-inactivating protein toxins, and it was found that the cytotoxicity in vitro increased up to 40,000 fold. They also showed an in vivo tumor response in murine fibrosarcomas after i.p. injection of toxin and local application of shock waves to the subcutaneous tumors. Our laboratory has previously used laser-generated shock waves to permeabilize cells in vitro (Lee et al., 1996; 1997; McAuliffe et al., 1997). It was shown (Lee et al., 1997) that erythrocytes were permeabilized by single shock waves from an ArF excimer laser. The explanation for the difference between these results and the present failure of laser-generated shock waves (including ArF excimer laser) to permeabilize HL60 cells, probably lies in marked differences between the membranes of the two cell types, although the pressure profile generated by the ArF laser (McAuliffe et al., 1997; Doukas et al., 1993, 1995) also showed differences from the present measured profile. Erythrocytes are known to have higher membrane fluidity (Feinstein et al., 1975; Van Blitterswijk et al., 1984), to be susceptible to the formation of plasma membrane pores after osmotic lysis (Lieber and Steck, 1982a, 1982b), and to have aquaporins or "water-channels" in the membrane, which have been implicated in the shock wave-induced permeability (Lee et al., 1997). In a previous paper (McAuliffe et al., 1997), we investigated the relationship between the number of laser-induced shock waves and the uptake of thymidine molecules. The uptake by two single shock waves was double that of a single shock wave. However, there was no significant difference between 2, 3, and 5 shock-wave exposures (the laser pulses were generated at 1 Hz). Further studies will be necessary to understand the mechanism of shock wave-induced uptake of drugs, focusing on the shock-wave impulse, the subsequent shear force against the cells, the change in membrane permeability of differing cell types, the applied number of shock waves, and the molecular size, ionic charge, and hydrophobicity of the drugs.

In the present paper, the survival fraction of the cells exposed to a single shock wave of 8.3–31.9 MPa was >0.95. Extracorporeal lithotripter-generated shock waves (measured in water) consist of a positive pressure component of 9–114 MPa and a negative pressure component of 2.8–9.9 MPa (Coleman and Saunders, 1989). From the previous in vitro results using lithotripter-generated shock waves, the LD_{50} varied between 250 and 400 shots at $P_+ =$ 24–50 MPa (Gambihler and Delius, 1992b; Miller and Thomas, 1995). In addition, there was no significant difference in the LD_{50} between normal and malignant cells (Brummer et al., 1990). Because the pressure profiles of lithotripter-generated shock waves are different from those in the present case, and the effect of cavitation bubbles has also been implicated in the mechanism of lithotripter-induced cell damage (Kodama and Takayama, 1998; Coleman and Saunders, 1993; Delius, 1994), the present data and the lithotripsy results cannot be directly compared.

When these pressure waves propagate in human tissue, side effects such as vascular damage and perirenal and intrarenal hematomas are induced (Delius, 1994; Brummer et al., 1990). In vivo reports have shown that hemorrhage occurs when shock waves are delivered to organs in the mouse. This has been observed in murine kidney (3–10 MPa, 5–200 shots) (Mayer et al., 1990; Raeman et al., 1994), in murine intestine (1–4 MPa, 100–200 shots) (Dalecki et al., 1995; Miller and Thomas, 1995), and in murine skin (0.6–1.6 MPa, 100 shots) (Miller and Thomas, 1995). Structural and histological damage was observed in rabbit liver after one shot obtained by detonating an explosive micropellet (<25 MPa) (Kodama et al., 1998). When rat liver was exposed to a single shock wave generated with the shock tube used in the present paper, both hemorrhage and structural damage were observed (data not shown).

Damage in vivo may be caused by shock-wave treatment consisting of lower pressure or fewer shocks, than that required to kill cells in vitro. That is, cells in vitro move with the surrounding liquid in the direction of the shock wave because the ratio of the density of the cell to that of liquid is close to one. The movement of the cell pellet in a polyethylene pipette exposed to a single shock wave was recorded with stroboscopic illumination (Brummer et al., 1989). Cells in vivo are fixed to neighboring cells, extracellular matrix, and basement membranes, and therefore show nonlinear, anisotropic and inhomogeneous behavior macroscopically. The tensile strength of human tissues can vary widely, for example, from 0.057 MPa for renal parenchyma, to 1.1–1.6 MPa for aorta, and 3.4 MPa for human cornea (Kitamura and Nangumo, 1978). Macroscopic tissue damage with shock waves may tend to occur with decreasing tensile strength of the tissue.

Shock waves can be focused deep within human bodies, using a reflector or acoustic lens with a large aperture to reduce the energy density along the shock wave path and to decrease pressure attenuation caused by viscous dissipation, which becomes significant for high frequencies. This procedure may have applications for localized delivery of plasmid DNA or oligonucleotides for gene therapy, and, in cancer therapy, by delivering molecules such as ribosome-inactivating protein toxins into tumors. However, it will be necessary to ensure that the shock-wave parameters needed

for effective cell permeabilization do not cause unacceptable tissue damage in vivo.

APPENDIX

In this section, expressions are derived for the relative displacement and the kinetic energy density difference between the cell and liquid phases due to an impulsive pressure. The cells are assumed to be uniformly distributed in the liquid.

The flow induced with an impulse pressure

Let the fluid be barotropic, so that the relation between the pressure p and the density ρ is given as

$$\int \frac{\mathrm{d}p}{\rho} = P(p), \tag{A1}$$

where P is the pressure function. Euler's equation of motion is given as

$$\begin{aligned} \frac{D\mathbf{v}}{Dt} &\equiv \frac{\partial \mathbf{v}}{\partial t} + (\mathbf{v}\cdot\mathrm{grad})\mathbf{v} \\ &= \mathbf{K} - \mathrm{grad}\, P, \end{aligned} \tag{A2}$$

where $\mathbf{K}$ is the sum of external and viscous forces.

When Eq. A2 is integrated over time t, from $t = 0$ to a short time τ, and finding the limit when $\tau \to 0$, the integral is

$$\mathbf{v} - \mathbf{v}_0 = \mathbf{G} - \mathrm{grad}\,\Pi, \tag{A3}$$

where $\mathbf{v}_0$ and $\mathbf{v}$ are the velocities immediately before and immediately after the change in the motion, and the impulsive, $\mathbf{G}$, and the impulsive pressure function, Π, are defined as (Imai, 1985)

$$\mathbf{G} = \lim_{\tau\to 0}\int_0^\tau \mathbf{K}\,\mathrm{d}t, \quad \Pi = \lim_{\tau\to 0}\int_0^\tau P\,\mathrm{d}t. \tag{A4}$$

The impulsive pressure function Π approaches infinity when $\tau \to 0$, and, consequently, $\mathbf{G}$ can be neglected. Assume that the fluid is initially at rest so that $\mathbf{v}_0 = 0$. The flow induced immediately after wave propagation is given as

$$\mathbf{v} = \mathrm{grad}\,\Phi, \quad \Phi = -\Pi. \tag{A5}$$

In the case of the incompressible fluid, $P = p/\rho$. The impulsive pressure, σ, is defined as

$$\sigma = \lim_{\tau\to 0}\int_0^\tau p\,\mathrm{d}t, \quad \Pi = \sigma/\rho. \tag{A6}$$

Hence,

$$v = \mathrm{grad}\,\Phi, \quad \sigma = -\rho\Phi. \tag{A7}$$

The kinetic energy is given as,

$$K = \frac{1}{2}\iint_S \sigma v_\mathrm{n}\,\mathrm{d}S, \quad \sigma = -\rho\Phi, \tag{A8}$$

where $\mathrm{d}S$ is the area element, and v_n denotes the velocity in the direction of the unit inward normal.

The relative motion between cells and fluid due to an impulsive pressure

Assume one-dimensional flow, and that the cells and the liquid are incompressible. Let the average density of the liquid including the cells be ρ_m, so that

$$\rho_\mathrm{m} = \alpha\rho_\mathrm{c} + (1-\alpha)\rho_\mathrm{f}, \tag{A9}$$

where α is the cellular volume fraction, ρ_c is the density of the cell phase, and ρ_f is the density of the liquid phase.

Consider the one-dimensional motion, which is induced with σ immediately. Let $v_{\mathrm{c}0}$ and $v_{\mathrm{f}0}$ be the immediate velocities of the single-phases of the cell and the liquid, respectively, which are produced by the impulsive pressure σ. From Eq. A7,

$$\rho_\mathrm{c} v_{\mathrm{c}0} = \rho_\mathrm{f} v_{\mathrm{f}0} = -\mathrm{grad}\,\sigma \tag{A10}$$

Suppose that the ratio of the volume of the cell phase to that of the liquid phase is given by α to $1-\alpha$, and each immediate velocity induced with σ is v_c and v_f, so that

$$\rho_\mathrm{c} v_\mathrm{c} = -\alpha\,\mathrm{grad}\,\sigma, \quad \rho_\mathrm{f} v_\mathrm{f} = -(1-\alpha)\mathrm{grad}\,\sigma. \tag{A11}$$

Using Eqs. A10 and A11,

$$v_\mathrm{c} = \alpha v_{\mathrm{c}0}, \quad v_\mathrm{f} = (1-\alpha)v_{\mathrm{f}0}. \tag{A12}$$

The impulsive relative velocity, w, between the cell and the liquid phases is given as

$$\begin{aligned} w &= v_\mathrm{c} - v_\mathrm{f} \\ &= \left(\frac{1-\alpha}{\rho_\mathrm{f}} - \frac{\alpha}{\rho_\mathrm{c}}\right)\mathrm{grad}\lim_{\tau\to 0}\int_0^\tau p\,\mathrm{d}t \\ &\approx \left(\frac{1-\alpha}{\rho_\mathrm{f}} - \frac{\alpha}{\rho_\mathrm{c}}\right)\frac{1}{\Delta x}\bar{p}\Delta t, \end{aligned} \tag{A13}$$

where Δt is the finite-time interval and $\bar{p}$ is the finite-time-averaged pressure.

Let the wave velocity of the impulsive pressure into the liquid with the cells be U_m, so that $U_\mathrm{m} = \Delta x/\Delta t$. Hence, Eq. A13 is written, using Eq. A9 as

$$w = \frac{\bar{p}}{\rho_\mathrm{m} U_\mathrm{m}}\left[\alpha(\beta-1)+1\right]\left[\left(1+\frac{1}{\beta}\right)\alpha - 1\right], \tag{A14}$$

where, $\beta = \rho_\mathrm{c}/\rho_\mathrm{f}$.

The difference in the kinetic energy density, ε_0, between the cell and the liquid phases is given as

$$\varepsilon_0 = -\frac{1}{2}\frac{\bar{p}^2}{\rho_\mathrm{m} U_\mathrm{m}^2}\left[\alpha(\beta-1)+1\right]\left[\left(1+\frac{1}{\beta}\right)\alpha - 1\right]. \tag{A15}$$

In the present paper, $\bar{p}$ is defined as

$$\bar{p} = \frac{1}{t_+}\int_0^{t_+} p(t)\,\mathrm{d}t = \frac{I}{t_+}, \tag{A16}$$

where I is the impulse and t_+ is the duration of positive pressure half-cycle given in Table 1.

Assuming that the pressure and density of the liquid including the cells are given by the Tait equation, then the wave velocity can be written as

$$U_m^2 = \frac{n(\bar{p} + B)}{\rho_m}. \quad \text{(A17)}$$

For water at 20°C, the constant B is given a value of 3.047×10^8 Pa, and the index n has the value 7.15 (Cole, 1948). The absolute relative displacement, $d(= w \times t_+)$, and absolute differences in the kinetic energy density, ε, between the cell and the liquid phases are given as

$$d = \left| \frac{I}{\rho_m U_m} [\alpha(\beta - 1) + 1] \left[\left(1 + \frac{1}{\beta} \right) \alpha - 1 \right] \right| \quad \text{(A18)}$$

$$\varepsilon = \left| -\frac{1}{2} \frac{I^2}{\rho_m U_m^2 t_+^2} [\alpha(\beta - 1) + 1] \left[\left(1 + \frac{1}{\beta} \right) \alpha - 1 \right] \right|. \quad \text{(A19)}$$

The authors wish to acknowledge J. Demirs, D. J. McAuliffe, S. Lee, and T. J. Flotte of the Wellman Laboratories of Photomedicine for their helpful discussions, and I. E. Kochevar for a critical reading of the manuscript. We are grateful to N. Michaud who recorded the confocal images.

T. Kodama was supported in part by the Cell Science Research Foundation, Japan. M. R. Hamblin was supported by the Office of Naval Research Medical Free Electron Laser Program (contract N 00014-94-1-0927). This work was partly supported by a contract from Mile Creek Capital, limited liability company, Boston, MA.

REFERENCES

Balhaus, W. F. J., and M. Holt. 1974. Interaction between the ocean surface and underwater spherical blast waves. *Phys. Fluids.* 17:1068–1079.

Barbieri, L., M. G. Battelli, and F. Stirpe. 1993. Ribosome-inactivating proteins from plants. *Biochim. Biophys. Acta.* 1154:237–282.

Basrai, M. A., F. Naider, and J. M. Becker. 1990. Internalization of lucifer yellow in *Candida albicans* by fluid phase endocytosis. *J. Gen. Microbiol.* 136:1059–1065.

Bohrer, M. P., W. M. Deen, C. R. Robertson, J. L. Troy, and B. M. Brenner. 1979. Influence of molecular configuration on the passage of macromolecules across the glomerular capillary wall. *J. Gen. Physiol.* 74:583–593.

Brummer, F., T. Brauner, and D. F. Hulser. 1990. Biological effects of shock waves. *World J. Urol.* 8:224–232.

Brummer, F., J. Brenner, T. Brauner, and D. F. Hulser. 1989. Effect of shock waves on suspended and immobilized L1210 cells. *Ultrasound Med. Biol.* 15:229–239.

Bushnell, J. C., and D. J. McCloskey. 1968. Thermoelastic stress production in solids. *J. Appl. Phys.* 39:5541–5546.

Cass, C. E., J. D. Young, and S. A. Baldwin. 1998. Recent advances in the molecular biology of nucleoside transporters of mammalian cells. *Biochem. Cell Biol.* 76:761–770.

Cockcroft, S. 1998. Phosphatidylinositol transfer proteins: a requirement in signal transduction and vesicle traffic. *Bioessays.* 20:423–432.

Cole, R. H. 1948. Underwater Explosions. Princeton University Press, Princeton, NJ. 36–45.

Coleman, A. J., and J. E. Saunders. 1989. A survey of the acoustic output of commercial extracorporeal shock wave lithotripters. *Ultrasound Med. Biol.* 15:213–227.

Coleman, A. J., and J. E. Saunders. 1993. A review of the physical properties and biological effects of the high amplitude acoustic field used in extracorporeal lithotripsy. *Ultrasonics.* 31:75–89.

Connelly, M. C., B. L. Robbins, and A. Fridland. 1993. Mechanism of uptake of the phosphonate analog (S)-1-(3-hydroxy-2-phosphonylmethoxypropyl)cytosine (HPMPC) in Vero cells. *Biochem. Pharmacol.* 46:1053–1057.

Curry, F. E., V. H. Huxley, and R. H. Adamson. 1983. Permeability of single capillaries to intermediate-sized colored solutes. *Am. J. Physiol. Heart Circ. Physiol.* 245:H495–H505.

Dalecki, D., C. H. Raeman, S. Z. Child, and E. L. Carstensen. 1995. Thresholds for intestinal hemorrhage in mice exposed to a piezoelectric lithotripter. *Ultrasound Med. Biol.* 21:1239–1246.

Delius, A., and G. Adams. 1999. Shock wave permeabilization with ribosome inactivating proteins: a new approach to tumor therapy. *Cancer Res.* 59:5227–5232.

Delius, M. 1994. Medical applications and bioeffects of extracorporeal shock waves. *Shock Waves.* 4:55–72.

Doukas, A. G., D. J. McAuliffe, and T. J. Flotte. 1993. Biological effects of laser-induced shock waves: structural and functional cell damage in vitro. *Ultrasound Med. Biol.* 19:137–146.

Doukas, A. G., D. J. McAuliffe, S. Lee, V. Venugopalan, and T. J. Flotte. 1995. Physical factors involved in stress-wave-induced cell injury: the effect of stress gradient. *Ultrasound Med. Biol.* 21:961–967.

Feinstein, M. B., S. M. Fernandez, and R. I. Sha'afi. 1975. Fluidity of natural membranes and phosphatidylserine and ganglioside dispersions. Effect of local anesthetics, cholesterol and protein. *Biochim. Biophys. Acta.* 413:354–370.

Finkel, T., and S. E. Epstein. 1995. Gene therapy for vascular disease. *Faseb. J.* 9:843–851.

Fox, J. R., and H. Wayland. 1979. Interstitial diffusion of macromolecules in the rat mesentery. *Microvasc. Res.* 18:255–276.

Frenz, M., G. Paltauf, and H. Schmidt-Kloiber. 1996. Laser-generated cavitation in absorbing liquid induced by acoustic diffraction. *Phys. Rev. Lett.* 76:3546–3549.

Fueyo, J., C. Gomez-Manzano, W. K. Yung, and A. P. Kyritsis. 1999. Targeting in gene therapy for gliomas. *Arch. Neurol.* 56:445–448.

Fung, Y. C. 1993. Biomechanics: Mechanical Properties of Living Tissues. Springer-Verlag, New York. 23–65.

Gambihler, S., and M. Delius. 1992a. Transient increase in membrane permeability of L1210 cells upon exposure to lithotripter shock waves in vitro. *Naturwissenschaften.* 79:328–329.

Gambihler, S., and M. Delius. 1992b. In vitro interaction of lithotripter shock waves and cytotoxic drugs. *Br. J. Cancer.* 66:69–73.

Gambihler, S., M. Delius, and J. W. Ellwart. 1994. Permeabilization of the plasma membrane of L1210 mouse leukemia cells using lithotripter shock waves. *J. Membr. Biol.* 141:267–275.

Glogauer, M., and C. A. McCulloch. 1992. Introduction of large molecules into viable fibroblasts by electroporation: optimization of loading and identification of labeled cellular compartments. *Exp. Cell Res.* 200: 227–234.

Gutierrez, A. A., N. R. Lemoine, and K. Sikora. 1992. Gene therapy for cancer. *Lancet.* 339:715–721.

Hall, J. G. 1958. Shock tubes, Part II: Production of strong shock waves; shock tube applications, design, and instrumentation. *Univ. Tor. Inst. Aerophys. Rev.* 12:142–163.

Hapala, I. 1997. Breaking the barrier: methods for reversible permeabilization of cellular membranes. *Crit. Rev. Biotechnol.* 17:105–122.

Ho, S. Y., and G. S. Mittal. 1996. Electroporation of cell membranes: a review. *Crit. Rev. Biotechnol.* 16:349–362.

IEC. 1998. IEC 61846, Ultrasonics—Pressure Pulse Lithotripters—Characteristics of fields. International Electrotechnical Commission, Geneva, Switzerland.

Imai, I. 1985. Fluid Dynamics. Vol 1. Syokabo Publishing Co., Ltd., Tokyo, Japan. 105–107.

Kambe, M., N. Ioritani, S. Shirai, K. Kambe, M. Kuwahara, D. Arita, T. Funato, H. Shimodaira, M. Gamo, S. Orikasa, and R. Kanamaru. 1996. Enhancement of chemotherapeutic effects with focused shock waves: extracorporeal shock wave chemotherapy (ESWC). *In Vivo.* 10: 369–375.

Kaneda, Y. 1999. Development of a novel fusogenic viral liposome system (HVJ-liposomes) and its applications to the treatment of acquired diseases. *Mol. Membr. Biol.* 16:119–122.

Kitamura, K., and T. Nangumo. 1978. Handbook of Biomedical Engineering. Corona Publishing Co. Ltd., Tokyo, Japan. 590–644.

Kodama, T., and K. Takayama. 1998. Dynamic behavior of bubbles during extracorporeal shock-wave lithotripsy. *Ultrasound Med. Biol.* 24: 723–738.

Kodama, T., H. Uenohara, and K. Takayama. 1998. Innovative technology for tissue disruption by explosive-induced shock waves. *Ultrasound Med. Biol.* 24:1459–1466.

Lee, S., T. Anderson, H. Zhang, T. J. Flotte, and A. G. Doukas. 1996. Alteration of cell membrane by stress waves in vitro. *Ultrasound Med. Biol.* 22:1285–1293.

Lee, S., and A. G. Doukas. 1999. Laser-generated stress waves and their effects on the cell membrane. *IEEE J. Sel. Top. Quant.* 5:997–1003.

Lee, S., D. J. McAuliffe, H. Zhang, Z. Xu, J. Taitelbaum, T. J. Flotte, and A. G. Doukas. 1997. Stress-wave-induced membrane permeation of red blood cells is facilitated by aquaporins. *Ultrasound Med. Biol.* 23: 1089–1094.

Lide, D. R. 1999. CRC Handbook of Chemistry and Physics. CRC Press LLC, Boca Raton, FL. 14–38.

Lieber, M. R., and T. L. Steck. 1982a. A description of the holes in human erythrocyte membrane ghosts. *J. Biol. Chem.* 257:11651–11659.

Lieber, M. R., and T. L. Steck. 1982b. Dynamics of the holes in human erythrocyte membrane ghosts. *J. Biol. Chem.* 257:11660–11666.

Liepman, H. W., and A. Roshko. 1957. Elements of Gas Dynamics. John Wiley and Sons Inc, New York. 62–83.

Liu, J., T. N. Lewis, and M. R. Prausnitz. 1998. Non-invasive assessment and control of ultrasound-mediated membrane permeabilization. *Pharm. Res.* 15:918–924.

Mayer, R., E. Schenk, S. Child, S. Norton, C. Cox, C. Hartman, C. Cox, and E. Carstensen. 1990. Pressure threshold for shock wave induced renal hemorrhage. *J. Urol.* 144:1505–1509.

McAuliffe, D. J., S. Lee, T. J. Flotte, and A. G. Doukas. 1997. Stress-wave-assisted transport through the plasma membrane in vitro. *Lasers Surg. Med.* 20:216–222.

Miller, D. L., S. Bao, and J. E. Morris. 1999. Sonoporation of cultured cells in the rotating tube exposure system. *Ultrasound Med. Biol.* 25:143–149.

Miller, D. L., and R. M. Thomas. 1995. Thresholds for hemorrhages in mouse skin and intestine induced by lithotripter shock waves. *Ultrasound Med. Biol.* 21:249–257.

Miller, D. L., A. R. Williams, J. E. Morris, and W. B. Chrisler. 1998. Sonoporation of erythrocytes by lithotripter shockwaves in vitro. *Ultrasonics.* 36:947–952.

Mir, L. M., H. Banoun, and C. Paoletti. 1988. Introduction of definite amounts of nonpermeant molecules into living cells after electropermeabilization: direct access to the cytosol. *Exp. Cell. Res.* 175:15–25.

Mukherjee, S., R. N. Ghosh, and F. R. Maxfield. 1997. Endocytosis. *Physiol. Rev.* 77:759–803.

Nugent, L. J., and R. K. Jain. 1984. Plasma pharmacokinetics and interstitial diffusion of macromolecules in a capillary bed. *Am. J. Physiol. Heart Circ. Physiol.* 246:H129–H137.

Paine, P. L., L. C. Moore, and S. B. Horowitz. 1975. Nuclear envelope permeability. *Nature.* 254:109–114.

Peters, R. 1984. Nucleo-cytoplasmic flux and intracellular mobility in single hepatocytes measured by fluorescence microphotolysis. *EMBO J.* 3:1831–1836.

Raeman, C. H., S. Z. Child, D. Dalecki, R. Mayer, K. J. Parker, and E. L. Carstensen. 1994. Damage to murine kidney and intestine from exposure to the fields of a piezoelectric lithotripter. *Ultrasound Med. Biol.* 20: 589–594.

Schafer, T., U. O. Karli, E. K. Gratwohl, F. E. Schweizer, and M. M. Burger. 1987. Digitonin-permeabilized cells are exocytosis competent. *J. Neurochem.* 49:1697–1707.

Schindler, M., and L. W. Jiang. 1986. Nuclear actin and myosin as control elements in nucleocytoplasmic transport. *J. Cell Biol.* 102:859–862.

Schwartz, R. S., S. Musto, M. E. Fabry, and R. L. Nagel. 1998. Two distinct pathways mediate the formation of intermediate density cells and hyperdense cells from normal density sickle red blood cells. *Blood.* 92:4844–4855.

Spiller, D. G., R. V. Giles, J. Grzybowski, D. M. Tidd, and R. E. Clark. 1998. Improving the intracellular delivery and molecular efficacy of antisense oligonucleotides in chronic myeloid leukemia cells: a comparison of streptolysin-O permeabilization, electroporation, and lipophilic conjugation. *Blood.* 91:4738–4746.

Steinbach, P., F. Hofstadter, H. Nicolai, W. Rossler, and W. Wieland. 1992. In vitro investigations on cellular damage induced by high energy shock waves. *Ultrasound Med. Biol.* 18:691–699.

Tennant, J. R. 1964. Evaluation of the trypan blue technique for determination of cell viability. *Transplantation.* 2:685–694.

Van Blitterswijk, W. J., H. Hilkmann, and T. Hengeveld. 1984. Differences in membrane lipid composition and fluidity of transplanted GRSL lymphoma cells, depending on their site of growth in the mouse. *Biochim. Biophys. Acta.* 778:521–529.

Weiss, N., M. Delius, S. Gambihler, H. Eichholtz-Wirth, P. Dirschedl, and W. Brendel. 1994. Effect of shock waves and cisplatin on cisplatin-sensitive and -resistant rodent tumors in vivo. *Int. J. Cancer.* 58: 693–699.